Modulated Resonant Transmission of Graphene Plasmons Across a λ/50 Plasmonic Waveguide Gap

Min Seok Jang,[1,*] Seyoon Kim,[1,2] Victor W. Brar,[3] Sergey G. Menabde,[1] and Harry A. Atwater[2,4]

[1] *School of Electric Engineering, Korea Advanced Institute of Science and Technology, Daejeon 34141, Korea*
[2] *Thomas J. Watson Laboratory of Applied Physics, California Institute of Technology, Pasadena, California 91125, USA*
[3] *Department of Physics, University of Wisconsin-Madison, Madison, Wisconsin 53706, USA*
[4] *Kavli Nanoscience Institute, California Institute of Technology, Pasadena, California 91125, USA*

(Received 7 June 2018; revised manuscript received 7 September 2018; published 26 November 2018)

We theoretically demonstrate the nontrivial transmission properties of a graphene-insulator-metal waveguide segment of deeply subwavelength scale. We show that, at midinfrared frequencies, the graphene-covered segment allows for the resonant transmission through the graphene-plasmon modes as well as the nonresonant transmission through background modes, and that these two pathways can lead to a strong Fano interference effect. The Fano interference enables a strong modulation of the overall optical transmission with a very small change in graphene Fermi level. By engineering the waveguide junction, it is possible that the two transmission pathways perfectly cancel each other out, resulting in a zero transmittance. We theoretically demonstrate the transmission modulation from 0% to 25% at 7.5-μm wavelength by shifting the Fermi level of graphene by a mere 15 meV. In addition, the active region of the device is more than 50 times shorter than the free-space wavelength. Thus, the reported phenomenon is of great advantage to the development of on-chip plasmonic devices.

DOI: 10.1103/PhysRevApplied.10.054053

I. INTRODUCTION

Graphene has been recently proposed as a candidate material for the electro-optic devices operating in mid-infrared that can control the phase and intensity of light at high data rates. The tunable light-graphene interaction can be achieved by controlling the graphene interband transitions [1–3] as well as by tuning the properties of the plasmon modes supported by the free carriers in a graphene sheet [4–6]. The graphene plasmons are particularly interesting for application purposes because the semimetallic and two-dimensional nature of graphene allows for these modes to be highly tunable and deeply subwavelength, with the plasmon wavelength shown to be around 100 times shorter than the free-space wavelength [7–9]. Furthermore, while the interband absorption efficiency of graphene is limited to a quantum of optical conductance (2.3%), the strong oscillator strength of the plasmonic modes allows for a higher dynamic range of control as well as more efficient light modulation within a smaller active area. These unconventional properties promise a creation of graphene-based active plasmonic devices that have high-modulation depth and can be integrated on a chip at length scales approaching those of electronic transistors.

Thus far, the plasmonically driven graphene nanoresonators have shown tunable absorption from terahertz to mid-infrared frequencies [10–16], and it has been experimentally demonstrated that the modulation depth can be significantly improved toward perfect modulation efficiencies when they are combined with noble metal plasmonic structures [15,16]. The graphene-plasmonic devices designed for the modulation of the free-space light have been mostly based on patterning a large number of quasi-identical resonators on a graphene sheet that supports plasmonic resonances that are collectively tuned by controlling the carrier density of the graphene sheet. Therefore, these devices have a large footprint (typically approximately 50×50 μm^2) and do not offer an opportunity to study single plasmonic cavity physics. In addition, the graphene Fermi level has to be tuned by a few hundred meV, which requires a large gate bias in order to completely shift the plasmon resonance into and out of the desired frequency range. Moreover, the Q factors of those devices are typically quite low (approximately 10) due to the edge roughness of the graphene ribbons caused by the lithography process [12,14–17]. Thus, while graphene ribbons of moderate mobility have been predicted to drive the total absorption with narrow resonance peaks, the extra loss introduced at the ribbon edges prevents such a performance from being experimentally observed.

*jang.minseok@kaist.ac.kr

In this work, we report on a device geometry that utilizes a single graphene-plasmonic cavity to actively tune the transmission through a metal-insulator-metal (*M-I-M*) waveguide. In this geometry, the transmission modulation is achieved via Fano interference effect, whereby the transmission through resonant graphene plasmons can destructively or constructively interfere with the transmission through nonresonant background modes. This mechanism provides multiple advantages over previously proposed structures. First, the proposed geometry utilizes the Fano interference property of being highly sensitive to the plasmonic resonance frequency of the graphene cavity, and thus a small variation of the graphene Fermi level (approximately 0.01 eV) creates a large change in the transmission intensity compared to the conventional graphene-based modulators solely utilizing the plasmon resonance or the interband transition in graphene. Second, we demonstrate an efficient light modulation with a single graphene cavity instead of using a large array of resonators [10–16] or an elongated waveguide structure [1–3] employed to enhance the optical response. This compact structure ensures a deeply subwavelength-device footprint, leading to an ultrafast and energy-efficient operation as well as providing means to study the single plasmon behavior in graphene such as nonlinear effects [18] and single-emitter coupling [4]. Finally, the graphene plasmons in our device are laterally confined by the graphene-metal interface rather than the physical edges of graphene, thus the fabrication of our device does not require a lithographic graphene patterning. Consequently, we expect that our device will avoid performance-limiting issues caused by patterned graphene, including the edge roughness and formation of the edge states [12,14–17], and therefore, could exhibit sharper plasmonic resonance compared to the previously demonstrated devices relying on the physically patterned graphene.

II. RESULTS AND DISCUSSION

A. Transmission through a composite plasmonic waveguide

A schematic of the device is shown in Fig. 1. Two identical *M-I-M* waveguides, consisting of a SiO_2 slab core and gold claddings, are separated by a small gap. In the gap region, the top gold layer is replaced with a sheet of graphene to form a short section of a graphene-insulator-metal (*G-I-M*) waveguide. The graphene layer is electrically grounded and its carrier density can be actively tuned by applying a gate voltage to the bottom gold layer. The thickness of the core d and the cladding h, and the size of the gap L are chosen as $d = h = 100$ nm and $L = 140$ nm. The operating photon energy of our device is chosen to be $\omega = 0.165$ eV, corresponding to the free-space wavelength λ_0 of 7.5 μm. This frequency is selected in order to suppress absorption losses due to the vibration modes in SiO_2

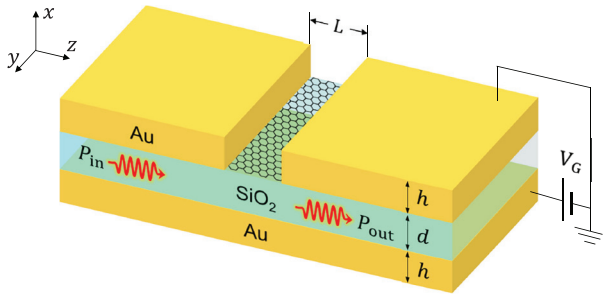

FIG. 1. Two identical *M-I-M* waveguides are separated by a narrow gap covered by a sheet of graphene. The thicknesses of the SiO_2 (d) and the gold h layers are both 100 nm, and the width of the gap L is 140 nm.

(approximately 0.133 eV) [19] and the optical phonons in graphene ($\geq$0.2 eV) [20], as well as to avoid plasmon-phonon coupling effects that are known to occur near the substrate phonon energies [21]. The input and output *M-I-M* waveguides support only the fundamental transverse magnetic mode (TM_0) because their thickness is far below the diffraction limit [22]. On the contrary, in the subwavelength gap region, there exist graphene plasmons, weakly bound surface plasmon polaritons (SPPs) on the bottom gold surface, and a continuum of unbound eigenmodes due to the semi-infinite free space above the graphene sheet.

In order to study the transmission properties of this composite waveguide structure, we begin by numerically investigating the coupling characteristics between *M-I-M* TM_0 and graphene plasmon modes across just a single *M-I-M–G-I-M* junction [Fig. 2(a)]. In this calculation, we obtain the steady-state solution of Maxwell's equations from full-wave simulations using the finite element method, and then decompose the total fields into the eigenmodes [21]. The optical properties of gold and SiO_2 are taken from Palik [19]. The graphene is considered as a thin film having a thickness of $\delta = 0.3$ nm and a dielectric function of $\epsilon_G = 1 + i\sigma/\omega\delta$. The optical conductivity of graphene $\sigma(\omega)$ is calculated within the local random-phase approximation [23], assuming a carrier mobility μ of 10 000 $cm^2\ V^{-1}\ s^{-1}$. The effective mode indices of *M-I-M* TM_0 (n_{M-I-M}) and graphene plasmons (n_G) are calculated to be $n_{M-I-M} = 1.11 + 0.033i$ and $n_G = 27.1 + 0.27i$ at Fermi energy $|E_F| = 0.4$ eV. Figure 2(a) shows the resulting steady-state electric-field profile when a TM_0 mode is continuously excited from the *M-I-M* waveguide and propagates to the *M-I-M–G-I-M* interface at $|E_F| = 0.4$ eV. The incident *M-I-M* TM_0 mode, which is launched from the left side, splits into a backward-propagating *M-I-M* TM_0 mode (reflection), forward-propagating graphene plasmons (transmission), and the background modes composed of unbound radiation and weakly bound gold SPPs.

We can characterize the mode-coupling relationship between the *M-I-M* TM_0 and the graphene-plasmon

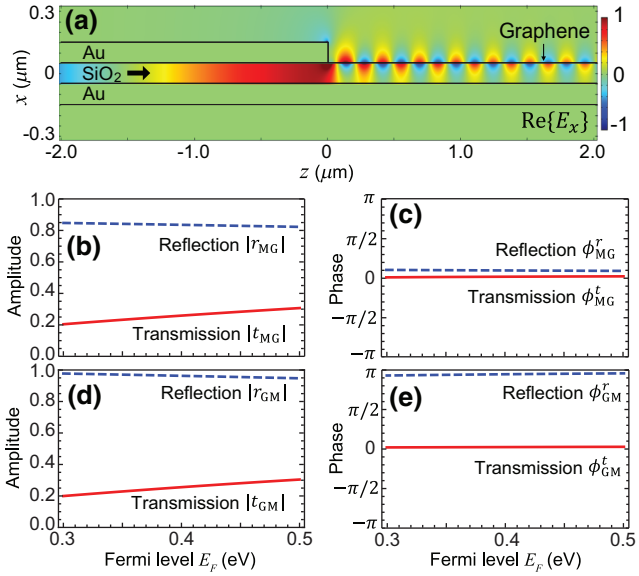

FIG. 2. (a) The electric-field distribution at the *M-I-M–G-I-M* junction at $E_F = 0.4$ eV. (b),(c) The amplitude and phase of the reflection (r_{MG}, blue dashed) and transmission (t_{MG}, red solid) coefficients for incoming *M-I-M* TM_0 mode as a function of graphene Fermi level. (d),(e) Same as (b),(c), but for the opposite geometry with the graphene plasmons propagating from the *G-I-M* segment into the *M-I-M* waveguide. The geometric parameters are chosen as $d = h = 100$ nm.

modes in the forward-propagating direction in terms of the complex transmission $t_{MG} = |t_{MG}|\exp(i\varphi^t_{MG})$ and reflection $r_{MG} = |r_{MG}|\exp(i\varphi^r_{MG})$ coefficients as shown in Figs. 2(b) and 2(c). Likewise, by launching the wave in the opposite direction, we can also calculate the $t_{GM} = |t_{GM}|\exp(i\varphi^t_{GM})$ and $r_{GM} = |r_{GM}|\exp(i\varphi^r_{GM})$ coefficients for incoming graphene plasmons hitting the *M-I-M* waveguide [Figs. 2(d) and 2(e)]. The amplitude of each coefficient is defined as $|t|^2 = P_t/P_i$ and $|r|^2 = P_r/P_i$, where P_i, P_t, and P_r are the time-averaged power flows carried by the incident, transmitted, and reflected modes, respectively. The phase term is determined such that $\varphi^{t,r} = \arg[E^{t,r}_x/E^i_x]$, where the complex electric-field components E^i_x, E^t_x, and E^r_x are evaluated at the junction. By comparing Figs. 2(b) and 2(d), a clear correspondence can be observed between the transmission coupling coefficients $|t_{MG}|^2$ and $|t_{GM}|^2$ from the *M-I-M* TM_0 to the graphene plasmon and from the graphene plasmon to the *M-I-M* TM_0, respectively. As the graphene Fermi level (E_F) is increased, the electromagnetic fields of the graphene-plasmon mode are less tightly confined to the graphene surface [20], and thus match better with the field profile of the TM_0 mode. As a result, their coupling efficiency rises from 4% to 9% as the Fermi level is varied from $E_F = 0.3$ eV to 0.5 eV. We also point out that $|r_{MG}|^2 + |t_{MG}|^2$ is only around 0.8, which indicates that almost 20% of the incident power carried by the *M-I-M* TM_0 mode is transferred to the background modes, which include the continuum of unbound radiation and the weakly bound gold surface plasmons. In contrast, the graphene plasmons do not significantly scatter into the background modes ($|r_{GM}|^2 + |t_{GM}|^2 \approx 1$). Finally, we note that the vertical air-metal interface at the waveguide junction imposes a π phase shift upon reflection of the graphene plasmon ($\varphi^r_{GM} \approx \pi$), but little phase change on the reflecting *M-I-M* TM_0 mode ($\varphi^r_{MG} \approx 0$), as shown in Figs. 2(c) and 2(e).

B. Fano interference between multiple modes in the gap

When two *M-I-M* waveguides are slightly separated from each other with a graphene-covered gap in between, a complex mode-coupling dynamics occurs between the guided *M-I-M* TM_0 mode and the gap modes. This effect produces a nontrivial Fermi-level dependence on the transmission from input to output ports. As shown in Fig. 3(a), the overall transmittance of an incident TM_0 wave in the *M-I-M–G-I-M–M-I-M* geometry now displays a number of sharp peaks and dips at particular E_F values. Most notably, the overall transmittance shows a sharp peak at $|E_F| = E_{max} = 0.38$ eV, but suddenly drops down and almost vanishes at $|E_F| = E_{min} = 0.395$ eV. The overall absorption and radiation loss in the active region of the device are also calculated and plotted in Fig 3(b). The absorption loss is calculated by integrating the ohmic power dissipation in graphene, and the radiation loss is obtained by integrating the Poynting vector of the

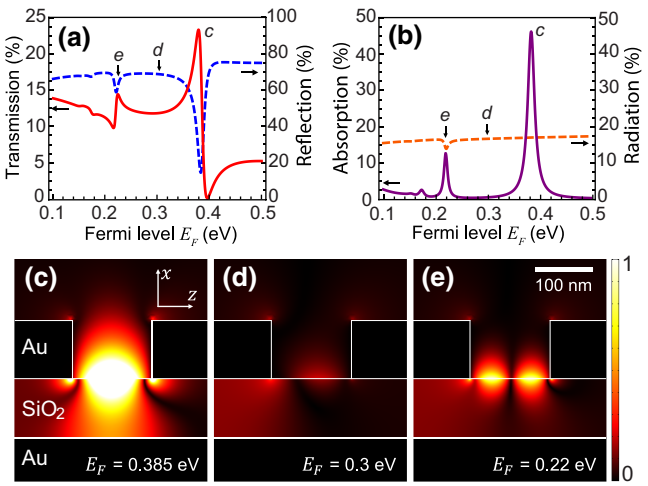

FIG. 3. (a),(b) The transmittance (red solid), reflectance (blue dashed), absorption (purple solid), and radiation loss (orange dashed) of the plasmonic modulator. The geometrical parameters are chosen as $d = h = 100$ nm and $L = 140$ nm. (c–e) The amplitude of the electric field $|E_x|$ at (c) $E_F = 0.385$ eV (the fundamental resonance mode), (d) at 0.3 eV (off resonance), and (e) at 0.22 eV (second-order resonance mode), all plotted in the same scale.

radiated waves directed to the upper-half space. Unlike the asymmetric line shape of transmission, the absorption exhibits a symmetric Lorentzian peak centered at $|E_F| = E_{\text{res}} = 0.385$ eV. Recognizing the fact that the major absorption occurs in the graphene layer, we attribute the absorption peak at $|E_F| = E_{\text{res}}$ to the Fabry-Perot resonances of graphene plasmons in the waveguide gap. By plotting the electric-field distribution of the device at 7.5 μm for E_F values corresponding to the absorption peaks [Figs. 3(c) and 3(e)], we find an intense, single node E field distribution at $|E_F| = 0.385$ eV, while for $|E_F| = 0.22$ eV, a double-node structure is revealed, indicating first- and second-order plasmonic resonances, respectively. In contrast, when the system is off resonance at $|E_F| = 0.3$ eV, the field concentration in the gap region is negligible, as exemplified in Fig. 3(d).

While the absorption of the *M-I-M–G-I-M–M-I-M* junction is associated with the Fabry-Perot resonance in the *G-I-M* cavity, the line shape of the overall transmission displayed in Fig. 3(a) requires an understanding of the multiple possible transmission pathways. The first transmission channel is through the resonant graphene-plasmonic mode, and its transmission coefficient, t_G, can be analytically obtained from the Fabry-Perot interferometer model in terms of the transmission and reflection coefficients at the *M-I-M–G-I-M* junction,

$$t_G = \frac{t_{\text{MG}} t_{\text{GM}} \exp(in_G k_0 L)}{1 - r_{\text{GM}}^2 \exp(2in_G k_0 L)},$$

where k_0 is the free-space wavenumber. As seen in Fig. 4(a), the amplitude of t_G exhibits a conventional symmetric-resonance curve centered at $|E_F| = 0.385$ eV that agrees well with the absorption maximum obtained from the full-wave simulations. The second transmission channel is through the background modes of the junction—both free-space modes and conventional metal-surface plasmons. The transmission coefficient through these modes, t_B, is calculated numerically, and approximated as a Femi-level independent constant t_B^0 as shown in Fig. 4(a).

Unlike the graphene-plasmon transmission, the background transmission is of a nonresonant nature, and slowly varies as a function of E_F in order to maintain eigenmodes' orthogonality in the waveguide as the variation in the graphene-plasmon mode alters the spatial profiles of the background modes. At the same time, the overall transmission across the *G-I-M* segment is highly dependent on the phase difference between the modes of two transmission channels. When the Fermi energy of graphene is lower than E_{res}, the t_B- and t_G-associated modes interfere constructively as they are roughly in phase, as shown in Fig. 4(b). The phase of the graphene-plasmon transmission is flipped by π across the resonance while the phase of the background transmission experiences little change, leading

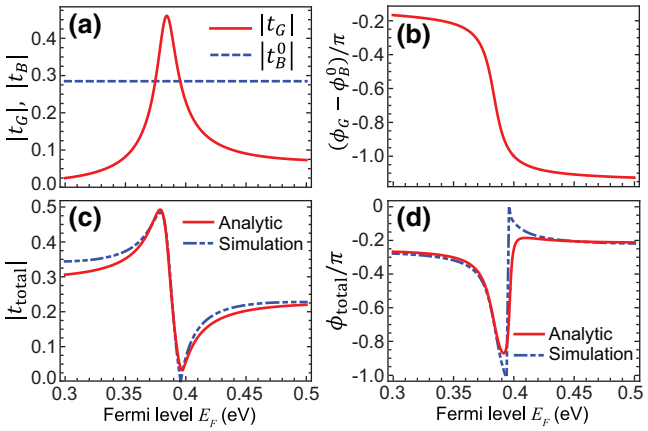

FIG. 4. (a) The amplitude of the transmission through the graphene-plasmon resonance (red solid), and through the background modes (blue dashed) vs E_F. (b) The phase difference between t_G and t_B^0, $\varphi_G - \varphi_B^0 = \arg(t_G) - \arg(t_B^0)$. (c),(d) The dependence of the amplitude and phase of the total transmission coefficient, $t_{\text{total}} = t_G + t_B$; the approximated analytic model (red) is in good accordance with the full simulation result (blue dashed) by capturing the distinctive asymmetric line shape.

to a destructive interference between two transmission processes for $E_F > E_{\text{res}}$. As a consequence, the maximum and minimum in overall transmission occur at either side of the plasmon resonance peak, producing the asymmetric-line shape as seen in Figs. 3(a) and 3(b).

In order to clearly illustrate the mechanism of this resonant interference, we provide an approximated analytic model in which we assume the background transmission as a Fermi energy-independent constant t_B^0. The value of t_B^0 is estimated as the average of total transmission coefficients at $E_F = 0.3$ and 0.5 eV, where the system is far off resonance, and thus the contribution from the plasmon transmission is minimal. The overall transmission coefficient is then obtained by simply adding both graphene-plasmon and background contributions, $t_G + t_B^0$. As shown in Fig. 4(b), the phase difference between two transmission channels varies from around -0.2π (constructive) to -1.2π (destructive) as E_F sweeps across E_{res}. Figures 4(c) and 4(d) show that the resulting analytic model has a strong correspondence with the full-wave simulation result, including the distinctive sharp-switching behavior. This type of resonant interference, which was first explained by Fano in the context of inelastic electron-scattering processes [24], generally occurs when a discrete state is embedded in a continuum [25,26]. In our structure, the discrete state is represented by the resonant graphene plasmons, while the continuum is represented by the background modes including the unbound radiations.

C. Modulation of the resonant transmission

The sharp-modulation behavior described above allows for large changes in transmission with very small changes

in graphene Fermi level ($\Delta E_F = 0.015$ eV), and therefore, requires a small variation of gate voltage for the switching operation. Estimated carrier-concentration difference between the maximum and minimum transmission states is $\Delta n = (E_{\mathrm{min}}^2 - E_{\mathrm{max}}^2)/\pi\hbar^2 v_F^2 \approx 8.5 \times 10^{11}$ cm^{-2}. The specific capacitance of the device is $C_G = 34.5$ nF/cm^2, leading us to the conclusion that the gate voltage ΔV_G one needs to apply between the bottom metal layer and graphene in order to switch the transmission from its minimum to maximum is only $\Delta V_G = e\Delta n/C_G \approx 3.96$ V. Moreover, the fundamental graphene-cavity mode involved in the resonant transmission has an extremely small mode volume. By conservatively assuming a diffraction-limited width [27] $W \sim \lambda_0$, where λ_0 is the free-space wavelength, the active volume of the device is approximated as $V \approx (d + 2h)LW \sim 10^{-3}\lambda_0^3$. This extreme miniaturization stems from the highly confined nature of the graphene plasmons. The small active area required for the resonant transmission along with superior electrical transport properties of graphene could result in an exceedingly short RC time constant, which, in principle, enables a fast switching speed.

The modulation intensity and the resonance condition of the device can be altered by engineering the geometry of the system. Most notably, the gap size L between the two M-I-M waveguides determines the Fermi energy at which the graphene plasmons are in resonance (E_{res}) at a given frequency [21]. From the dispersion relation of graphene plasmons [10,28] $\omega \propto E_F^{1/2} k_G^{1/2}$, where $k_G = n_G k_0$ is the wavenumber of the graphene plasmon, we deduce that an increasing gap size L lowers the resonance frequency at a fixed Fermi energy, but raises E_{res} at a fixed frequency. At the same time, the devices with wider gaps show higher modulation intensity as presented in Figs. 5(a) and 5(b), because higher E_{res} induces stronger plasmon resonance as the coupling of the M-I-M TM_0 to the graphene plasmons becomes more efficient (Fig. 2). The thickness of the metal cladding h and the dielectric core d of the M-I-M waveguides do not significantly alter the resonance Fermi energy, but affect the transmission characteristics by modulating the relative phase and intensities of the graphene-plasmon transmission and the background transmission. Thickening the metal cladding h of the M-I-M waveguides monotonically increases the maximum overall transmission T_{max} by suppressing the radiative loss and enforcing the background transmission. While a thicker dielectric core d is also favorable for higher background transmission, the thicker core broadens the M-I-M-guided mode, resulting in worse spatial-mode matching with the graphene plasmons, deteriorating t_G. The dependence of T_{max} on d is, therefore, nonmonotonic, as summarized in Fig. 5(c).

We emphasize that the overall transmission can be entirely suppressed by inducing total destructive interference between the graphene-plasmon and background transmissions, $t_G = -t_B$. This condition for the zero transmission can be achieved by carefully adjusting the geometrical parameters of the system. The maximum amplitude of the graphene plasmon transmission at resonance should be greater than the background transmission ($|t_G(E_{\mathrm{res}})| > |t_B|$), and their phase difference $\varphi_G - \varphi_B$ should also be controlled by tuning the mode-coupling characteristics at the waveguide junctions. Figure 5(d) plots the simulated ratio of the maximum and minimum transmission $T_{\mathrm{max}}/T_{\mathrm{min}}$ as a function of the core thickness d and the cladding thickness h. Indeed, the on/off ratio diverges for a certain set of parameter values as indicated in Fig. 5(d), showing that the complete suppression of transmission is achievable.

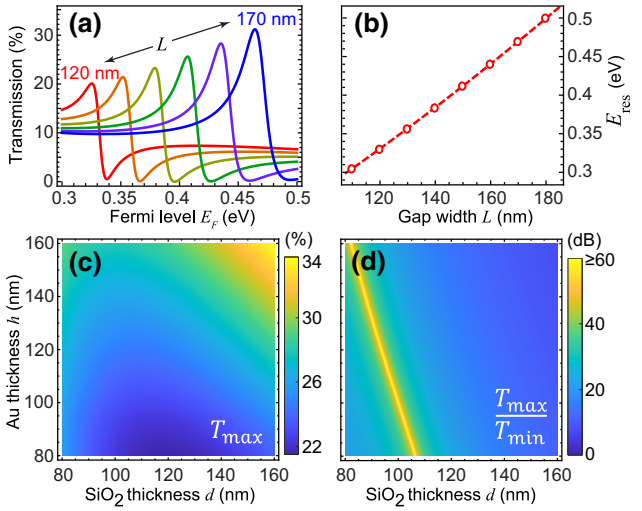

FIG. 5. (a) The transmittance T vs E_F for the gap size L from 120 nm (red) up to 170 nm (blue) with a 10-nm step; here, the transmittances are obtained from full-wave simulations using the finite element method. (b) Dependence of E_{res} on L; the analytically obtained E_{res} (red dashed) perfectly agrees with the FEM simulation results (red circles). (c) The maximum transmittance T_{max}, and (d) the ratio of the maximum and minimum transmittance $T_{\mathrm{max}}/T_{\mathrm{min}}$ plotted as a function of d and h. The $T_{\mathrm{max}}/T_{\mathrm{min}}$ values over the 60 dB correspond to the total destructive interference between the resonant (graphene) and nonresonant (background) transmission. In (c) and (d), L is set to 140 nm as in the cases of Fig. 3.

D. Modulation efficiency dependence on the graphene quality

As a final remark, we discuss how the overall transmission depends on the carrier mobility of graphene. Since the propagation loss of graphene plasmons is inversely proportional to its carrier mobility [20], we calculate the transmittance as varying the carrier mobility of graphene μ from 10^3 to 10^5 cm^2 V^{-1} s^{-1} depending on the fabrication method [29–31] and the substrate material [32,33]. Figure 6(a) shows that T_{max} can be as high as 50% for $\mu = 5 \times 10^4$ cm^2 V^{-1} s^{-1} and decreases down to 11% at $\mu = 1000$ cm^2 V^{-1} s^{-1}. In Fig. 6(b), the minimum nearly

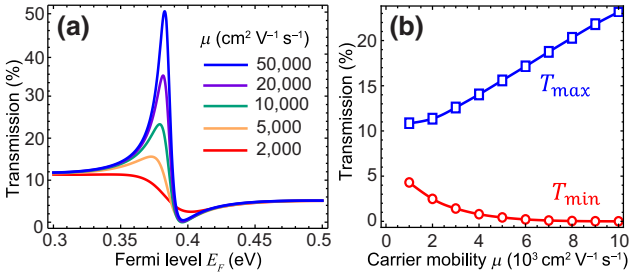

FIG. 6. (a) The transmittance T vs E_F for different carrier mobility μ (as denoted). (b) Dependence of $T_{\max}$ (blue squares) and $T_{\min}$ (red circles) on μ.

vanishes for $\mu \geq 5000\,\mathrm{cm^2\,V^{-1}\,s^{-1}}$, which corresponds to the condition of $|t_G(E_{\mathrm{res}})| \geq |t_B|$. The $T_{\max}/T_{\min}$ ratio is predicted to be 2.5 times lower for a low-quality graphene of $\mu = 1000\,\mathrm{cm^2\,V^{-1}s^{-1}}$.

III. CONCLUSION

In summary, we propose a graphene-based mid-infrared plasmonic waveguide modulator, which exhibits a sharp resonant transmission coming from the Fano interference between the plasmon resonance in graphene and the background transmission. In the proposed device, the resonant interference between the graphene-plasmon transmission and the background transmission can entirely suppress the overall transmission, resulting in a very high-modulation efficiency, which requires a very small change in the graphene Fermi level (on the order of 10 meV) for switching. Moreover, the active volume of the device is about a thousand times smaller than the diffraction limit, making it a promising building block for deep-subwavelength ultrafast optical-integrated devices.

ACKNOWLWDGMENTS

The authors acknowledge support from the National Research Foundation of Korea (NRF) (Grant No. 2017R1E1A1A01074323, M.S.J.) and KAIST Global Center for Open Research with Enterprise (GCORE) (Grant No. N11180017, S.G.M.) funded by the Ministry of Science and ICT, and Basic Science Research Program through NRF funded by the Ministry of Education (Grant No. 2017R1D1A1B03034762, M.S.J). M.S.J., V.W.B., and H.A.A. acknowledge support from the Air Force Office of Scientific Research through Grant No. FA9550-16-1-0019. V.W.B. thanks the Wisconsin Alumni Research Foundation for support.

M.S.J., and S.K. contributed equally to this work

[1] M. Liu, X. Yin, E. Ulin-Avila, B. Geng, T. Zentgraf, L. Ju, F. Wang, and X. Zhang, A graphene-based broadband optical modulator, Nature **474**, 64 (2011).

[2] C. T. Phare, Y.-H. D. Lee, J. Cardenas, and M. Lipson, Graphene electro-optic modulator with 30 GHz bandwidth, Nat. Photonics **9**, 511 (2015).

[3] V. Sorianello, M. Midrio, G. Contestabile, I. Asselberghs, J. Van Campenhout, C. Huyghebaert, I. Goykhman, A. K. Ott, A. C. Ferrari, and M. Romagnoli, Graphene–silicon phase modulators with gigahertz bandwidth, Nat. Photonics **12**, 40 (2018).

[4] F. H. L. Koppens, D. E. Chang, and F. J. García de Abajo, Graphene plasmonics: A platform for strong light–matter interactions, Nano Lett. **11**, 3370 (2011).

[5] A. N. Grigorenko, M. Polini, and K. S. Novoselov, Graphene plasmonics, Nat. Photonics **6**, 749 (2012).

[6] F. J. García de Abajo, Graphene plasmonics: Challenges and opportunities, ACS Photonics **1**, 135 (2014).

[7] J. Chen, M. Badioli, P. Alonso-González, S. Thongrattanasiri, F. Huth, J. Osmond, M. Spasenović, A. Centeno, A. Pesquera, P. Godignon, A. Z. Elorza, N. Camara, F. J. García de Abajo, R. Hillenbrand, and F. H. L. Koppens, Optical nano-imaging of gate-tunable graphene plasmons, Nature **487**, 77 (2012).

[8] Z. Fei, A. S. Rodin, G. O. Andreev, W. Bao, A. S. McLeod, M. Wagner, L. M. Zhang, Z. Zhao, M. Thiemens, G. Dominguez, M. M. Fogler, A. H. Castro Neto, C. N. Lau, F. Keilmann, and D. N. Basov, Gate-tuning of graphene plasmons revealed by infrared nano-imaging, Nature **487**, 82 (2012).

[9] P. Alonso-González, A. Y. Nikitin, F. Golmar, A. Centeno, A. Pesquera, S. Vélez, J. Chen, G. Navickaite, F. Koppens, A. Zurutuza, F. Casanova, L. E. Hueso, and R. Hillenbrand, Controlling graphene plasmons with resonant metal antennas and spatial conductivity patterns, Science **344**, 1369 (2014).

[10] L. Ju, B. Geng, J. Horng, C. Girit, M. Martin, Z. Hao, H. A. Bechtel, X. Liang, A. Zettl, Y. R. Shen, and F. Wang, Graphene plasmonics for tunable terahertz metamaterials, Nat. Nanotechnol. **6**, 630 (2011).

[11] S. Thongrattanasiri, F. H. L. Koppens, and F. J. García de Abajo, Complete Optical Absorption in Periodically Patterned Graphene, Phys. Rev. Lett. **108**, 047401 (2012).

[12] H. Yan, T. Low, W. Zhu, Y. Wu, M. Freitag, X. Li, F. Guinea, P. Avouris, and F. Xia, Damping pathways of mid-infrared plasmons in graphene nanostructures, Nat. Photonics **7**, 394 (2013).

[13] V. W. Brar, M. S. Jang, M. Sherrott, J. J. Lopez, and H. A. Atwater, Highly confined tunable mid-infrared plasmonics in graphene nanoresonators, Nano Lett. **13**, 2541 (2013).

[14] M. S. Jang, V. W. Brar, M. C. Sherrott, J. J. Lopez, L. Kim, S. Kim, M. Choi, and H. A. Atwater, Tunable large resonant absorption in a midinfrared graphene Salisbury screen, Phys. Rev. B **90**, 165409 (2014).

[15] S. Kim, M. S. Jang, V. W. Brar, Y. Tolstova, K. W. Mauser, and H. A. Atwater, Electronically tunable extraordinary optical transmission in graphene plasmonic ribbons coupled to subwavelength metallic slit arrays, Nat. Commun. **7**, 12323 (2016).

[16] S. Kim, M. S. Jang, V. W. Brar, K. W. Mauser, L. Kim, and H. A. Atwater, Electronically tunable perfect absorption in graphene, Nano Lett. **18**, 971 (2018).

[17] Z. Fei, M. D. Goldflam, J.-S. Wu, S. Dai, M. Wagner, A. S. McLeod, M. K. Liu, K. W. Post, S. Zhu, G. C. A. M.

Janssen, M. M. Fogler, and D. N. Basov, Edge and surface plasmons in graphene nanoribbons, Nano Lett. **15**, 8271 (2015).

[18] M. Gullans, D. E. Chang, F. H. L. Koppens, F. J. García de Abajo, and M. D. Lukin, Single-Photon Nonlinear Optics with Graphene Plasmons, Phys. Rev. Lett. **111**, 247401 (2013).

[19] E. D. Palik, *Handbook of Optical Constants of Solids* (Academic Press, New York, 1998).

[20] M. Jablan, H. Buljan, and M. Soljacic, Plasmonics in graphene at infrared frequencies, Phys. Rev. B **80**, 245435 (2009).

[21] See Supplemental Material at http://link.aps.org/supplemental/10.1103/PhysRevApplied.10.054053 for details on the electromagnetic simulation methods, optical conductivity of graphene, and discussion of the operation frequency window and graphene plasmon resonance.

[22] M. Born and E. Wolf, *Principles of Optics: Electromagnetic Theory of Propagation, Interference and Diffraction of Light* (Cambridge University Press, Cambridge, 1999).

[23] L. A. Falkovsky and A. A. Varlamov, Space-time dispersion of graphene conductivity, Eur. Phys. J. B **56**, 281 (2007).

[24] U. Fano, Effects of configuration interaction on intensities and phase shifts, Phys. Rev. **124**, 1866 (1961).

[25] B. Luk'yanchuk, M. I. Zheludev, S. A. Maier, N. J. Halas, P. Nordlander, H. Giessen, and C. T. Chong, The Fano resonance in plasmonic nanostructures and metamaterials, Nat. Mater. **9**, 707 (2010).

[26] E. Miroshnichenko, S. Flach, and Y. S. Kivshar, Fano resonances in nanoscale structures, Rev. Mod. Phys. **82**, 2257 (2010).

[27] S. A. Maier, Effective mode volume of nanoscale plasmon cavities, Opt. Quant. Electron. **38**, 257 (2006).

[28] E. H. Hwang and S. D. Sarma, Dielectric function, screening, and plasmons in two-dimensional graphene, Phys. Rev. B **75**, 205418 (2007).

[29] S. Park and R. S. Ruoff, Chemical methods for the production of graphenes, Nat. Nanotechnol. **5**, 217 (2010).

[30] J. Kim, H. Park, J. B. Hannon, S. W. Bedell, K. Fogel, D. K. Sadana, and C. Dimitrakopoulos, Layer-resolved graphene transfer via engineered strain layers, Science **342**, 833 (2013).

[31] J. H. Lee, E. K. Lee, W. J. Joo, Y. Jang, B. S. Kim, J. Y. Lim, S. H. Choi, S. J. Ahn, J. R. Ahn, M. H. Park, C. W. Yang, B. L. Choi, S. W. Hwang, and D. Whang, Wafer-scale growth of single-crystal monolayer graphene on reusable hydrogen-terminated germanium, Science **344**, 286 (2014).

[32] K. I. Bolotin, K. J. Sikes, J. Hone, H. L. Stormer, and P. Kim, Temperature-Dependent Transport in Suspended Graphene, Phys. Rev. Lett. **101**, 096802 (2008).

[33] C. R. Dean, A. F. Young, I. Meric, C. Lee, L. Wang, S. Sorgenfrei, K. Watanabe, T. Taniguchi, P. Kim, K. L. Shepard, and J. Hone, Boron nitride substrates for high-quality graphene electronics, Nat. Nanotechnol. **5**, 722 (2010).